Available online at www.sciencedirect.com
SCIENCE DIRECT®
Remote Sensing of Environment 103 (2006) 369–378
Remote Sensing of Environment
www.elsevier.com/locate/rse

A multi-scale analysis of dynamic optical signals in a Southern California chaparral ecosystem: A comparison of field, AVIRIS and MODIS data

Yufu Cheng [a,*], John A. Gamon [a], David A. Fuentes [a], Zhiyan Mao [a], Daniel A. Sims [b], Hong-lie Qiu [c], Helen Claudio [a], Alfredo Huete [d], Abdullah F. Rahman [b]

[a] Department of Biological Sciences, California State University LA, Los Angeles, CA 90032, United States
[b] Department of Geography, Ball State University, Muncie, IN 47306, United States
[c] Department of Geography and Urban Analysis, California State University LA, Los Angeles, CA 90032, United States
[d] Department of Soil, Water and Environ. Sciences, University of Arizona, Tucson, AZ 85721-0038, United States

Received 13 May 2004; received in revised form 23 June 2005; accepted 23 June 2005

Abstract

Using field data, Airborne Visible Infrared Imaging Spectrometer (AVIRIS) imagery, and Moderate-Resolution Imaging Spectroradiometer (MODIS) data, a multi-scale analysis of ecosystem optical properties was performed for Sky Oaks, a Southern California chaparral ecosystem in the spectral network (SpecNet) and FLUXNET networks. The study covered a 4-year period (2000–2004), which included a severe drought in 2002 and a subsequent wildfire in July 2003, leading to extreme perturbation in ecosystem productivity and optical properties. Two vegetation greenness indices (Normalized Difference Vegetation Index (NDVI) and Enhanced Vegetation Index (EVI)), and a measure of the fraction of photosynthetically active radiation absorbed by vegetation (fPAR), were compared across sampling platforms, which ranged in pixel size from 1 m (tram system in the field) to 1000 m (MODIS satellite sensor). The three MODIS products closely followed the same seasonal trends as the tram and AVIRIS data, but tended to be higher than the tram and AVIRIS values, particularly for fPAR and NDVI. Following a wildfire that removed all green vegetation, the overestimation in MODIS fPAR values was particularly clear. The MODIS fPAR algorithm (version 4 vs. v.4.1) had a significant effect on the degree of overestimation, with v. 4.1 improving the agreement with the other sensors (AVIRIS and tram) for vegetated conditions, but not for low, post-fire values. The differences between MODIS products and the products from the other platform sensors could not be entirely attributed to differences in sensor spectral responses or sampling scale. These results are consistent with several other recently published studies that indicate that MODIS overestimates fPAR and thus net primary production (NPP) for many terrestrial ecosystems, and demonstrates the need for proper validation of MODIS terrestrial biospheric products by direct comparison against optical signals at other spatial scales, as is now possible at several SpecNet sites. The study also demonstrates the utility of in-situ field sampling (e.g. tram systems) and hyperspectral aircraft imagery for proper interpretation of satellite data taken at coarse spatial scales.

Keywords: Validation; Scale; MODIS; AVIRIS; Field measurement; NDVI; EVI; fPAR; Disturbance (wildfire, drought); Chaparral

1. Introduction

An understanding of scaling effects is critical if we are to properly interpret remotely sensed signals gathered at different temporal and spatial scales (Lobo et al., 1997; Roberts, 2001; Salomonson & Appel, 2004; Tian et al., 2003; Wu & Strahler, 1994). Satellite sensors provide large spatial patterns with regional or global coverage (Chen, 1999). However, the coarse resolution of satellite sensors are problematic, particularly for patchy landscapes (Turner et al., 2003). To properly validate and interpret satellite imagery, additional remotely sensed and biophysical data (e.g. ground truthing or aircraft imagery) are needed (Chen et al., 2002; Lakshmi & Zehrfuhs, 2002; Peddle et al., 2004; Reich et al., 1999; Turner et al., 2003). For example, aircraft or field imagery at fine spatial scales (e.g. 1 m to 100 m) can be used to extrapolate to coarse resolution data at large scales (e.g. 1 km). However, the spatial scale difference

* Corresponding author. Tel.: +1 323 343 4224; fax: +1 323 343 6451.
E-mail address: ycheng5@exchange.calstatela.edu (Y. Cheng).

0034-4257/$ - see front matter © 2006 Elsevier Inc. All rights reserved.
doi:10.1016/j.rse.2005.06.013

between satellite and ground measurements present several challenges for comparing measurements made across vastly different scales (Aman et al., 1992; Gao et al., 2001; Lakshmi & Zehrfuhs, 2002; Smith & Ballard, 1999).

There are many difficulties associated with cross-scale comparisons. Area difference of different sensors require area-weighting operations (Gitelson, 2004; Soegaard et al., 2000), and different sensor algorithms are used to derive vegetation indices and associated products (Chen, 1999). Furthermore, surface heterogeneity causes key ecosystem processes to vary with spatial scale (Chen, 1999). Additionally, each sensor or algorithm has its own inherent error, which should be considered in any cross-sensor comparison, but is often difficult to assess directly. While fraught with many challenges, an explicit comparison of different sampling scales provides a useful means to validate satellite signals (e.g. MODIS products). Such comparison can give confidence to calculations of regional and global carbon budgets, or can indicate problems in these calculations (or their underlying inputs or assumptions) that need further improvement. Furthermore, multi-scale analyses can indicate causes of variation at different scales in optical properties that help reveal the controls of the ecosystem carbon and water vapor fluxes for different ecosystems (Ehleringer et al., 2002; Rahman et al., 2001; Schimel et al., 2001; Wang et al., 2004).

The development of appropriate ground-based validation techniques is critical to evaluate uncertainties associated with satellite data-based products. Recently, validation studies suggest considerable errors exist in some of the MODIS products. Of primary concern are the LAI and fPAR products, because they form the basis of most global models of terrestrial productivity (Fensholt et al., 2004). Recently, studies from several different ecosystems reported that MODIS fPAR differed from field data, with most ecosystems showing over-estimation of fPAR by MODIS (Fensholt et al., 2004; Huemmrich et al., 2005; Turner et al., 2005). Recent studies have also reported similar disagreements between MODIS-derived LAI and independently derived LAI estimates from models and ground-based measurements (Fensholt et al., 2004; Huemmrich et al., 2005; Wythers et al., 2003).

This overestimation of fPAR or LAI by MODIS has consequences for subsequent primary productivity (GPP and NPP) products, which depend on fPAR or LAI, as well as incident PAR, temperature and vapor pressure deficit (Reich et al., 1999; Turner et al., 2003). Indeed, several reports have indicated similar errors in MODIS primary productivity estimates. Recently, MODIS gross primary productivity (GPP) products have been compared with scaled GPP estimates (25 km^2) derived from ground measurements at two forested sites by the Bigfoot project research team (Reich et al., 1999; Turner et al., 2003). This analysis revealed a mismatch between MODIS GPP products versus ground-based GPP due to both fPAR and light use efficiency differences (Reich et al., 1999; Turner et al., 2003); MODIS GPP products tended to be higher (2 to 5 $gC\ m^{-2}\ day^{-1}$ more) than ground measurements (Turner et al., 2003). Rahman et al. (2004) reported overestimation of MODIS GPP from a deciduous forest site in Indiana, with an inability to capture the seasonal patterns during spring growth and fall leaf drop. More recently, Turner et al. (2005) reported that the degree of fidelity between field-based and MODIS-based GPP and NPP varied considerably across ecosystems, with MODIS GPP and NPP estimates being consistently low at some sites (e.g. agricultural ecosystems) and high at others (desert grassland and dry coniferous forest sites).

These recent findings indicate that further testing of MODIS products against field-derived data is needed before we can have confidence in these satellite products. Since the issue of accuracy is often clouded by the fact that we are comparing different sensors or sampling methods operating at vastly different spatial scales, there is a need to develop standardized "scaling methods" for comparing satellite data to field data. Further, there is some indication in the recent literature that MODIS may tend to overestimate in dry or semi-arid sites (Turner et al., 2005). Thus, the objective of this paper is to present an approach for comparing optical signals for a single chaparral ecosystem using data from sensors at three different scales: satellite (MODIS), aircraft (AVIRIS) hyperspectral images and field (tram) measurements as a basis for satellite validation. The primary focus of this study is on three optical indices, NDVI, EVI and fPAR. The continuous dataset from this site, spanning extreme wet and dry periods as well as a wildfire, provides a unique opportunity to compare results across platforms over a wide range of conditions. We present and evaluate a method for linking coarse scale satellite data (1 km pixel sizes) to fine scale field measurements (1 m pixel sizes) by using hyperspectral aircraft imagery as an intermediate scaling tool (Fig. 1).

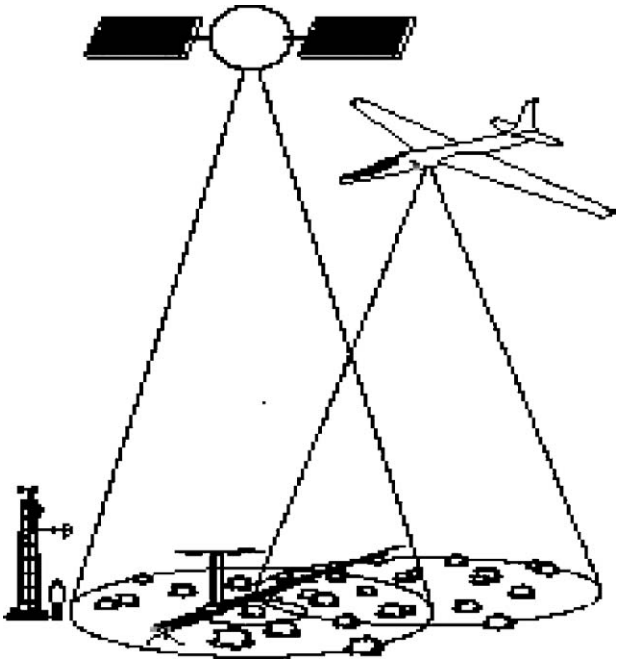

Fig. 1. Illustration of multi-scale sampling methods employed in this study. At the top, the satellite sensor (MODIS) provides regional to global coverage with large (1000 m) pixel sizes). In the middle, the aircraft sensor (AVIRIS) can provide images with an intermediate range of pixel sizes allowing us to compare ecosystem optical properties at different scales. At the bottom, an automated mobile spectrometer (tram system) provides periodic sampling of surface optical properties along a 100-m transect, closely matched to the scale of a flux tower footprint.

2. Materials and methods

2.1. Site

The study was conducted at the Sky Oaks Biological Field Station (33°23′N, 116°37′W) of San Diego State University, located in southern California, at approximately 1420 m in elevation and 75 km east of the Pacific Ocean. The site consists of a chaparral stand that was previously burnt in 1898 (Marion & Black, 1988) and recently burnt in July 2003. *Adenostoma fasciculatum*, a dominant species in California chaparral, was also the dominant species at this site. Other major shrubs included *Adenostoma sparsifolium* and *Ceanothus greggi* (Keeley, 1992). The site experiences a Mediterranean climate, characterized by cool, wet winters and hot, dry summers, and winter rainfall is periodically increased or decreased by El Niño and La Niña events, respectively, providing tremendous interannual variability in productivity.

3. Data

3.1. MODIS data

MODIS "cutout" surface reflectance and vegetation indices (version 4) for Sky Oaks, California, were downloaded from the Oaks Ridge National Lab's database at http://public.ornl.gov/fluxnet/modis.cfm. The data from pixel 33 (a 1 km^2 pixel including the flux tower and tram, Fig. 2) of a 7 by 7 pixel array were extracted to construct a time series for comparison with the same variables derived from AVIRIS and tram data. The NDVI and EVI were 16-day composites and the fPAR was an 8-day composite. The MODIS Quality Assurance values associated with each date were used to evaluate the MODIS data quality, with most dates rated "best possible," in part reflecting the excellent clear-sky conditions typical of this arid site. The NDVI and EVI from MODIS were calculated as follows:

$$\mathrm{NDVI} = \frac{\rho_{\mathrm{NIR}} - \rho_{\mathrm{Red}}}{\rho_{\mathrm{NIR}} + \rho_{\mathrm{Red}}} \quad (1)$$

$$\mathrm{EVI} = G^{*} \frac{\rho_{\mathrm{NIR}} - \rho_{\mathrm{Red}}}{\rho_{\mathrm{NIR}} + C_1\rho_{\mathrm{Red}} - C_2\rho_{\mathrm{Blue}} + L} \quad (2)$$

where,

ρ_{NIR}	Near infrared reflectance
ρ_{Red}	Red reflectance
ρ_{Blue}	Blue reflectance
C_1	Atmosphere resistance red correction coefficient
C_2	Atmosphere resistance blue correction coefficient
L	Canopy background brightness correction factor
G	Gain factor

where $L=1$, $C_1=6$, $C_2=7.5$, $G=2.5$ (Huete et al., 1994, 1997).

MODIS 8-day fPAR (MOD15A2, both version 4 and 4.1) was obtained from Boston University's FTP server. To derive this dataset, the MODIS fPAR main algorithm was developed using three-dimensional radiative transfer theory (Myneni et al., 2002). A look-up table approach was used with an inverse model based on a land cover (six major biomes) map at 1 km spatial resolution (Knyazikhin et al., 1998)). The model used several fixed parameters characterizing a certain biome along with vegetation structural information, soil brightness, and meteorological input (precipitation and air temperature) for the biome (Myneni et al., 1997)). MODIS surface reflectance was compared to model-based results in look-up tables to derive all possible solutions for fPAR (Knyazikhin et al., 1998)). The archived fPAR product was the mean of the distribution functions (Knyazikhin et al., 1998)). When this method failed to find a solution (mainly due to cloudy conditions), a back-up algorithm based on the NDVI–fPAR relationship was applied (Myneni et al., 1997). In this dataset, only one data point was derived from back up algorithm (Julian day 353 in 2003).

Note that our original analysis was conducted using MODIS fPAR version 4, and in the course of this study, an error in the version 4 fPAR code was discovered, requiring us to repeat the analysis with version 4.1 fPAR, which improved the agreement with fPAR derived from the other sensors. Consequently, our primary study conclusions derive from the improved version 4.1 (unless otherwise noted, all figures present MODIS version 4.1 fPAR data). However, since previously published studies (Fensholt et al., 2004; Huemmrich et al., 2005) have reported results from earlier fPAR versions, we chose to include a comparison of algorithm version in our analysis (see Fig. 8, and Results and Discussion).

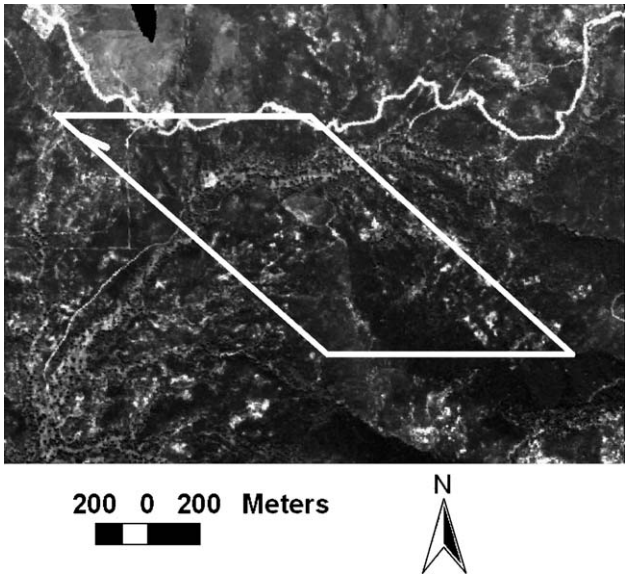

Fig. 2. The MODIS pixel (1 km^2 parallelogram) overlaid on the AVIRIS hyperspectral image at Sky Oaks in Southern California. Sky Oaks tram system is located at the upper left corner of the MODIS "cutout" pixel. The parallelogram shape of the MODIS pixel results from overlaying the MODIS ISIN projection over the standard UTM projection applied to the hyperspectral AVIRIS image.

3.2. AVIRIS

The Airborne Visible Infrared Spectrometer (AVIRIS) acquires hyperspectral data between 400 and 2400 nm with an approximate bandwidth of 10 nm (Green et al., 1998). For

this study, a total of five available images were analyzed between April 2002 and September 2003, with pixel sizes ranging from 2.3 to 15.8 m, depending upon flight altitude. The time frame of AVIRIS flights was during mid-day (10:00 to 14:00), the same time period as the MODIS and tram data to facilitate comparison. AVIRIS radiance images were converted to surface reflectance using the radiative transfer software ACORN (Goetz et al., 2003) (ImSpec LLC, WA, USA). To compare AVIRIS optical signals to the MODIS pixel and the tram sampling regions, the AVIRIS pixels matching the locations of the tram and MODIS sampling regions were extracted separately for analysis. Vegetation indices were calculated from the averaged reflectance derived from these separate regions of the AVIRIS images. The reflectance was interpolated to 1 nm intervals using a linear interpolation method with commercial software (ENVI, Research Systems, Inc, CO, USA). The NDVI and fPAR were calculated from the averaged AVIRIS image reflectance as follows:

$$\mathrm{NDVI} = \frac{(R_{800} - R_{680})}{(R_{800} + R_{680})} \quad (3)$$

$$\mathrm{fPAR} = 1.24 \times \mathrm{NDVI} - 0.168 \quad (4)$$

The fPAR equation (Eq. (4)) was a relationship derived empirically by comparing NDVI values to field measured fPAR values for a large range of southwestern vegetation ($R^2 = 0.95$, Sims et al., 2006-this issue). In this relationship, a correction was applied for the green area fraction of the vegetation, eliminating any confounding contribution of non-photosynthetic vegetation components (e.g. stems or dead leaves) to the fPAR. Additionally, MODIS-simulated NDVI and EVI values were calculated from AVIRIS. To do this, the spectral region between 400 and 1000 nm from AVIRIS reflectance images was interpolated to 1 nm intervals. Since there are multiple channels for each MODIS band and these channels have slightly different relative spectral responses (RSR), we resampled each channel's RSR to 1 nm intervals, and then averaged them together to create an average RSR function for each band. To calculate the MODIS band reflectance from hyperspectral data, we summed the product of the average RSR and the input reflectance spectrum and normalized this by the sum of the average RSR as follows:

$$\text{Band reflectance} = \Sigma(\text{RSR*Input reflectance}) / \Sigma(\text{RSR}) \quad (5)$$

Eqs. (1) and (2) were applied to calculate MODIS-simulated NDVI and EVI.

3.3. Tram system

The ground reflectance measurements were collected with an automated, dual-channel hyperspectral spectrometer (UniSpecDC, PP Systems, Amesbury, MA). Most data were collected with the spectrometer mounted on a mobile "Tram system" that provided repeated samplings of the same 100 m transect. This system consisted of a robotic cart mounted on an elevated track. However, before the tram was constructed (May 2001), and briefly after the tram was destroyed by fire (July 2003), data were collected by manual measurement along the identical 100-m transect. The ground resolution ("pixel size") for each tram measurement was roughly 1 m^2, but ranged from 0.75 to 1.80 m^2 depending on the height of the tram track, which varied along the 100-m transect with topography. The tram system provided the advantages of repeated and automated sampling, allowing us to sample the identical transect on the ground through time. The dual detector spectrometer, with upwelling and downwelling detectors, provided real-time correction of sky conditions, allowing for atmospherically corrected surface reflectance even under cloudy conditions. Tram reflectance data were processed to reflectance using software (MultiSpec, available at http://vcsars.calstatela.edu/lab_documents/mspec.html) that interpolated wavebands to 1-nm intervals. The NDVI and fPAR used in this analysis were calculated through the Eqs. (3) and (4) from averaged surface reflectance along the 100 m transect. Additionally, MODIS-simulated NDVI and EVI values were also calculated from tram data for comparison to MODIS's vegetation indices products using the same methods described in the AVIRIS data section.

4. Results

4.1. Surface reflectance

Noticeable differences were apparent in the reflectance spectra obtained from MODIS, AVIRIS and the tram system. Tram reflectance values tended to be higher across most wavelengths than either AVIRIS or MODIS, and MODIS reflectance values tended to be lower, particularly for the pre-burn data (Fig. 3A). The AVIRIS reflectance spectra varied slightly depending upon the footprint sampled (tram transect or MODIS pixel), and yielded higher values for the tram region than for the full MODIS pixel. The July 2003 fire caused the reflectance spectra from all sensors to flatten at the red edge (around 700 nm) due to the loss of green vegetation. Differences in reflectance spectra among instruments were reduced by the fire, demonstrating that some of the variation between instruments was due to heterogeneous vegetation cover across the different sampling regions.

4.2. NDVI

A comparison of NDVI values between sensors revealed effects of both sampling scale and NDVI formulation (Fig. 4). The MODIS NDVI followed similar temporal patterns as the AVIRIS and the tram data, but were consistently higher than the tram NDVI values. AVIRIS NDVI values varied with sampling footprint (tram transect or MODIS pixel). When simulating the tram transect, AVIRIS NDVI (dark triangles in Fig. 4) yielded excellent agreement with the tram NDVI values. When simulating the MODIS pixel (open triangles, Fig. 4), AVIRIS NDVI more closely approximated the MODIS values (i.e. were higher than the tram NDVI values) but were not as high as the

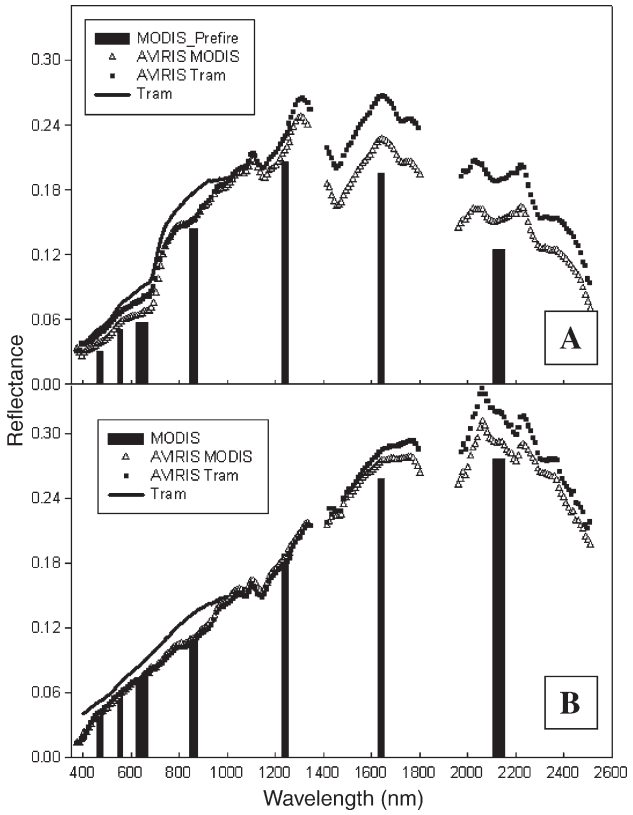

Fig. 3. MODIS, AVIRIS and Tram reflectance before fire (average of four available data sets from all the platforms on 4/13/2002, 7/19/2002, 9/23/2002 and 3/7/2003) (panel A) and postfire (on 9/16/2003) (panel B). AVIRIS reflectance is shown for two sampling regions: 1) an area matching the MODIS pixel ("AVIRIS MODIS") and 2) an area matching the tram transect ("AVIRIS tram").

NDVI obtained from the MODIS pixel. When MODIS-simulated NDVI values were calculated from tram and AVIRIS data (instead of the narrow-band NDVI from Eq. (3)), there was better agreement between the sensors, particularly after the fire (Fig. 4, right panel), confirming that part of the differences between sensors was attributable to NDVI formulation. However, MODIS NDVI values were still higher than either the tram or AVIRIS NDVI values. Thus, it appeared that even after considering spatial scale and NDVI formulation, some residual effect remained, causing MODIS NDVI values to be consistently higher than aircraft or tram data, particularly for vegetated surfaces.

4.3. EVI

EVI exhibited remarkably good agreement across sensors and sampling scales, but with considerably more "noise" than NDVI (Fig. 5). The EVI from all the platforms showed clear effects of season, drought and fire. With the exception of occasional high "spikes" in the MODIS EVI values and a couple of low AVIRIS EVI values during the drought period, all sensors yielded nearly identical patterns and magnitudes of EVI, even across these extreme perturbations. MODIS quality flags revealed that most EVI values used in the analysis were from nominally clear days only, the "spikes" for MODIS EVI might be due to MODIS residual cloud contamination, view angles, or the atmospheric correction (Huete et al., 2002). The general agreement among sensors suggests that automated field data (tram) can provide suitable validation for properly corrected image data from aircraft and satellite.

4.4. fPAR

Both before and after the fire, AVIRIS fPAR values for the tram area (solid triangles, Fig. 6) were indistinguishable from the tram values. Similarly, before the fire, AVIRIS fPAR values for the MODIS pixels were in close agreement with the MODIS fPAR value, both in seasonal patterns and magnitudes, with MODIS fPAR values being slightly higher than AVIRIS fPAR (hollow triangles, Fig. 6). However, after the fire, MODIS fPAR values were much higher than both the tram and AVIRIS values.

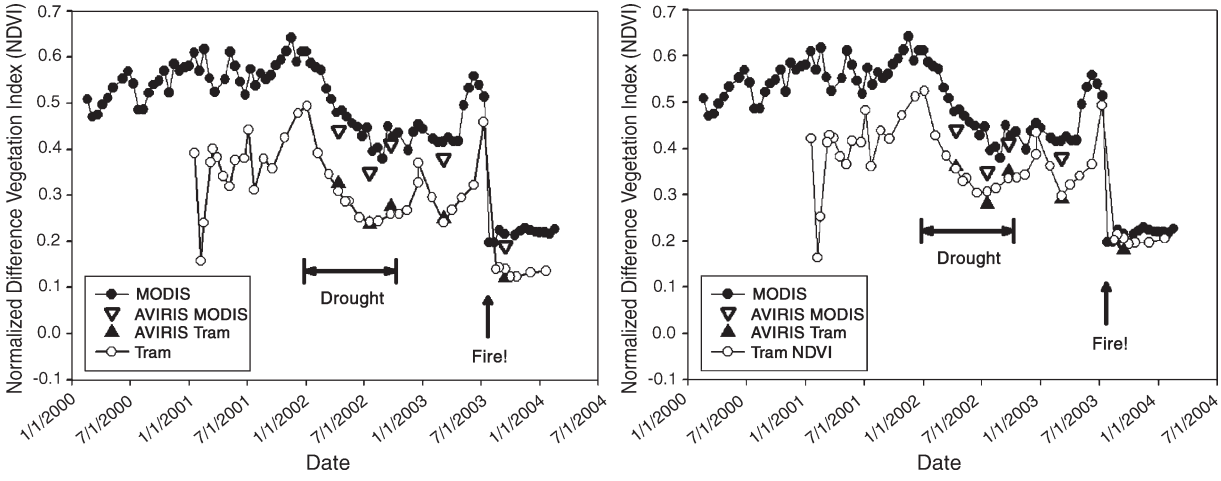

Fig. 4. Comparison of the Normalized Difference Vegetation Index (NDVI) calculated from MODIS (Sky Oaks cutout pixel 33, which overlapped the tram region as shown in Fig. 2), AVIRIS and the Sky Oaks tram system. In the left panel, the NDVI from the tram system and AVIRIS are calculated using Eq. (3). In the right panel, the NDVI from the tram system and AVIRIS are calculated using MODIS-simulated NDVI. The hollow down triangle denotes NDVI derived from the AVIRIS image region matching the entire MODIS pixel. The solid triangle denotes NDVI derived from the AVIRIS image region matching the tram transect. Note the close agreement between AVIRIS and the tram, but not between MODIS and the tram.

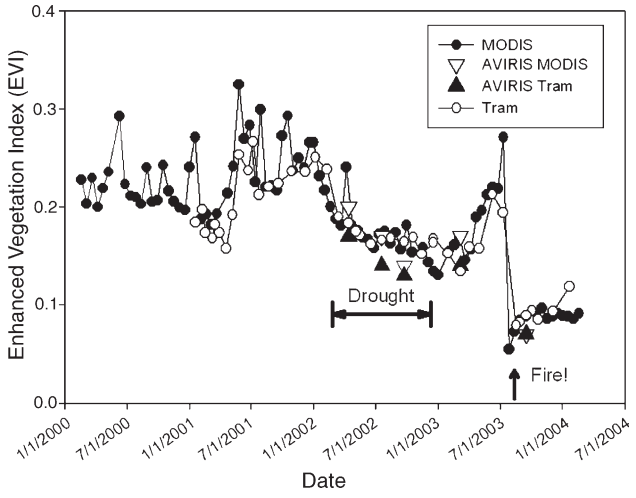

Fig. 5. Comparison of the Enhanced Vegetation Index (EVI) calculated from MODIS, AVIRIS and the Sky Oaks tram system. The hollow down triangle denotes that EVI was derived for the AVIRIS image matching the entire MODIS pixel. The solid triangle denotes that EVI was derived from the AVIRIS image region matching the tram transect. Note the close agreement among EVI values from all platforms.

At this time, when virtually no green vegetation remained on the landscape, MODIS yielded high fPAR values (with an average of 0.15 for MODIS, versus the more believable tram values of approximately zero). The AVIRIS fPAR varied slightly with the sampling footprint. When simulating the tram transect, AVIRIS fPAR values (solid triangles, Fig. 6) were in exact agreement with tram values. When simulating the MODIS pixel (open triangles, Fig. 6) AVIRIS fPAR values were slightly higher than the tram values, but not as large as the MODIS fPAR values. Thus, it appears that the current MODIS 4.1 fPAR algorithm overestimates fPAR for this site, particularly after fire, which would lead to subsequent errors in biospheric products related

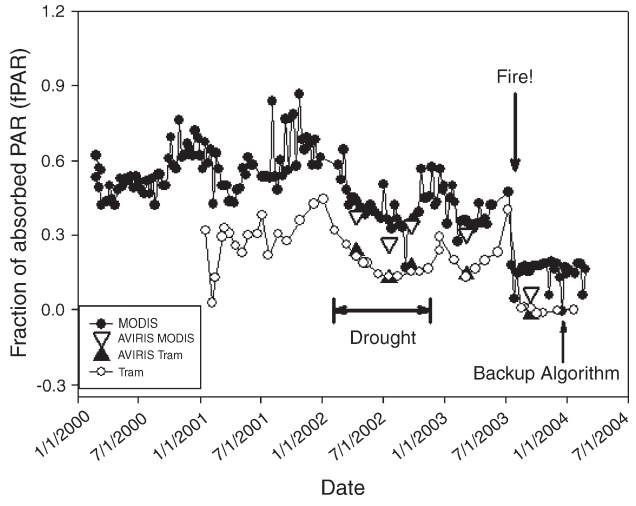

Fig. 6. Comparison of the fraction of absorbed Photosynthetically Active Radiation (fPAR) calculated from MODIS, AVIRIS and the Sky Oaks tram system. The hollow triangle denotes fPAR derived for the AVIRIS image region matching the entire MODIS pixel. The solid triangle denotes fPAR derived from the AVIRIS image region matching the tram transect. MODIS fPAR derived by backup algorithm was indicated by up arrow (one data point only).

to fPAR (e.g. net primary productivity). Interestingly, the single fPAR value (indicated by an arrow in Fig. 6), obtained from the backup algorithm involving derivation of fPAR directly from NDVI, was much lower than the fPAR values from the standard MODIS algorithm and was indistinguishable from the tram data.

In the course of this study, we observed even larger differences between MODIS version 4 fPAR and field-based fPAR from our study (not shown). This overestimation was considerably reduced when we repeated this analysis with version 4.1 fPAR suggesting that earlier versions of the MODIS fPAR algorithm may have tended to overestimate fPAR values relative to direct field data.

The comparison of NDVI, EVI and fPAR across sampling platforms is summarized in Fig. 7, which provides pairwise comparisons between AVIRIS-derived indices (*X*-axis) and either the MODIS or tram-derived indices (*Y*-axis), with the 1:1 line provided as a reference. Note that for the two regressions in

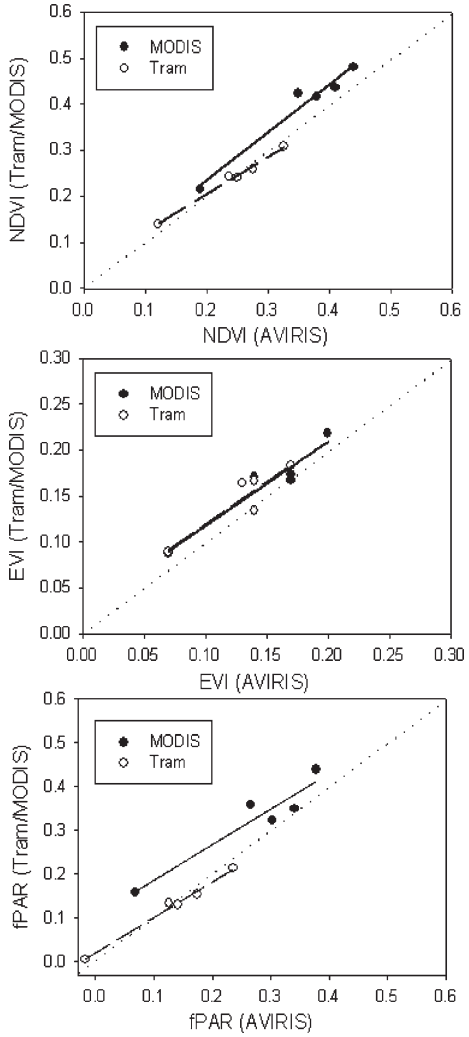

Fig. 7. Pair-wise comparisons between AVIRIS and either tram (open circles) or MODIS (closed circles) indices (NDVI, EVI, and fPAR). The 1:1 line is provided as a reference (dotted line). In these comparisons, the AVIRIS values were derived from regions of interest matching the MODIS (close symbols) or tram (open symbols) sampling regions.

each figure, the AVIRIS values were calculated from contrasting AVIRIS footprints (matching either the MODIS or the tram sampling footprint). Several points can be concluded from these pairwise comparisons. The regression line comparing AVIRIS and MODIS NDVI is slightly above the 1:1 line, supporting the conclusion of a slight overestimation by MODIS NDVI. In contrast, the regression line comparing AVIRIS and tram NDVI are indistinguishable from the 1:1 line, indicating good agreement between these sensors and platforms. For EVI, both regressions (AVIRIS-MODIS and AVIRIS-tram) are slightly above the 1:1 line, with the two regression lines are indistinguishable from each other. This reflects the very close agreement between tram and MODIS EVI (also evident in Fig. 5), and indicates that the AVIRIS EVI values are slightly lower than either the tram or MODIS EVI values. For fPAR, the AVIRIS-MODIS regression falls above the 1:1 line, and this is particularly clear for the lowest fPAR value (the post-fire value), when no green vegetation was present. By contrast, the AVIRIS-tram regression is indistinguishable from the 1:1 line, indicating good agreement between these the fPAR derived from these two platforms. The degree of scatter in these regressions (summarized by the R^2 and p values, Table 1), provide some indication of the fidelity between values across platforms over widely varying conditions (wet and dry years, and pre- and post-fire). For all comparisons, the close agreement across sampling platforms (indicated by high R^2 values and low p values) indicates that all sensors and indices are closely following the seasonal and interannual variability in ecosystem productivity. Particularly remarkable is the very close agreement between the tram and AVIRIS NDVI and fPAR values (indicated by high R^2 values, low p values, and overlap with the 1:1 line).

The effect of MODIS fPAR algorithm version is illustrated in Fig. 8, which compares the v. 4 to the v. 4.1 MODIS fPAR collections across all dates for this site. Particularly at high fPAR values (when green vegetation was present on the landscape), the earlier (v. 4) fPAR collection yielded very high values, which were considerably reduced in the newer (v. 4.1) fPAR collection. However, there was little change for low fPAR values (indicating post-fire data, when no green vegetation was present on the landscape). This comparison reveals a significant impact of the MODIS algorithm version on fPAR, which may partly explain the tendency for MODIS fPAR to over-estimate fPAR for a variety of terrestrial ecosystems around the world (Turner et al., 2003).

Table 1
Regression statistics for Fig. 7

Indices	Items	Tram	MODIS
NDVI	Slope	0.8097	1.0394
	Intercept	0.0422	0.0268
	R^2	0.9909	0.9647
	P-value	0.0004	0.0029
EVI	Slope	0.9231	0.9167
	Intercept	0.0274	0.0257
	R^2	0.8382	0.9280
	P-value	0.0291	0.0084
fPAR	Slope	0.8097	0.8125
	Intercept	0.0204	0.1052
	R^2	0.9909	0.9068
	P-value	0.0004	0.0124

In each regression, AVIRIS values are compared to corresponding values for either the tram or MODIS sensors.

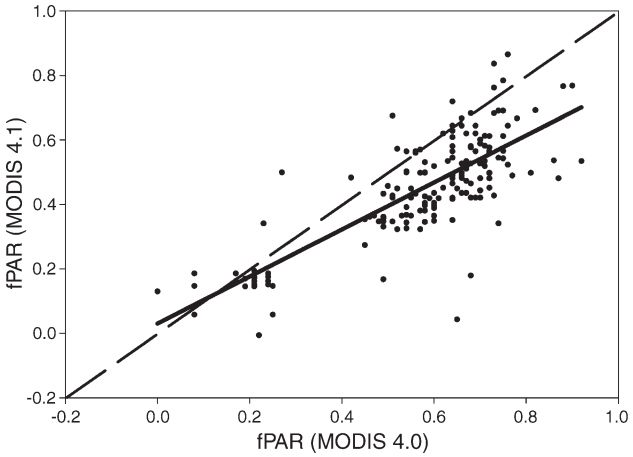

Fig. 8. Comparison of MODIS fPAR versions 4.0 vs. 4.1 for our study site. Note that version 4.1 reduced the fPAR values, particularly for high fPAR values, but did not change the low (post-fire) values appreciably.

5. Discussion

The results presented here clearly illustrate some of the challenges faced by comparing optical data across vastly different spatial scales (1 m pixels to 1000 m pixels, a difference of 3 orders of magnitude), and the value of a multi-scale sampling approach to bridging these vastly different scales. MODIS data and tram data yielded remarkably similar temporal patterns in NDVI, EVI, and fPAR. However, the higher MODIS NDVI and fPAR values suggest that these MODIS products are currently overestimated in some situations, and thus may be resulting in abnormally high NPP estimates. Our findings of high MODIS NDVI and fPAR values are in agreement with other recent validation efforts (Turner et al., 2003), and suggest that errors remain in the current MODIS algorithms for these terrestrial biospheric products. The reasons for these errors remain unclear, largely due to the relatively small numbers of validation efforts to date, the various MODIS algorithm versions used, and due to the obvious difficulties in validating such large-scale (1000 km) pixels, which greatly exceed the scale of most field based measurements. Additionally, in the composite (8- or 16-day products) many of the possible error sources are invisible to the end user. That, along with the evolving nature of the MODIS algorithms, along with their inherent complexity, makes it difficult to track exact sources of error. However, the results presented here provide some insight into the cause of this disagreement.

The use of the AVIRIS data to simulate both tram and MODIS data enabled us to explore the potential causes of difference between MODIS and tram data. The different sampling regions of the tram and MODIS could partly explain the higher MODIS NDVI and FPAR values; using AVIRIS to

simulate the MODIS pixel area increased the NDVI and fPAR values slightly over the tram values, but not enough to fully explain the even higher MODIS values. Similarly, applying the identical MODIS NDVI formula to tram and AVIRIS data brought the NDVI values from the three platforms closer together, but still could not fully explain the higher MODIS NDVI and the very high fPAR values after the disturbance. Thus, we conclude that there are unidentified errors remaining in the MODIS processing that result in the overestimation of NDVI and fPAR.

It is possible that errors in atmospheric correction could partly explain the slightly higher MODIS NDVI values relative to the other sensors. Overcorrection for atmospheric scattering could cause artificially low red reflectance values and lead to high NDVI values, which is consistent with the results shown in Figs. 3 and 4. Additionally, other sensor calibration, design, background noise, or sampling issues (e.g. viewing angle) may be factors in the slightly higher MODIS NDVI values. These possibilities cannot be directly evaluated in the final MODIS composite products, which represent the sum of many data processing decisions made by several MODIS processing teams. Thus, a full evaluation of these possibilities is beyond the scope of this study. Further studies should focus on isolating the various possible reasons for the high NDVI values obtained with the MODIS sensor by looking at each step in the data processing stream.

The EVI appeared to be relatively scale-independent in that it yielded the best agreement between the tram and MODIS platforms. Presumably, this is because EVI reduces errors caused by atmospheric scattering and soil background (Huete et al., 2002), both of which were potential error sources in our study. However, the cause of the noise in the EVI data (high spikes, particularly in the earlier MODIS data) remains unclear. Similarly, the reason for the slightly lower AVIRIS EVI values relative to the tram and MODIS remains unclear, but could be partly due to the different atmospheric correction approaches used for the different sensor platforms. Previous studies have shown that MODIS EVI worked well in a highly disturbed, burned areas through a dark target-based atmospheric correction with MODIS surface reflectance data (Miura et al., 2001). The comparison of EVI with NDVI indicates that background correction is very important, especially for landscapes with open canopies, which includes desert and shrubland such as this semi-arid chaparral site (Huete et al., 2002). EVI has the additional benefit of not saturating as easily as NDVI for ecosystem with a high leaf area index (Gao & Li, 2000) or with high chlorophyll levels (Xiao et al., 2004), but it is not clear that this benefit had any relevance in this relatively sparse chaparral stand. Further study should focus on the relative merits of NDVI and EVI across a range of spatial scales and ecosystems.

Since fPAR is the basis for the terrestrial NPP products (Nemani et al., 2003), overestimation of fPAR would necessarily lead to overestimation of NPP, as has been recently reported for an eastern deciduous forest (Rahman et al., 2004). The most troubling finding of this study is apparent overestimation of fPAR by MODIS after fire. After the fire, the MODIS fPAR product was approximately 0.15 (15%), a remarkably high value for a burned area having an fPAR of essentially zero, which was confirmed by both tram and AVIRIS measurements. The overestimation of MODIS fPAR was particularly noticeable in earlier MODIS products (version 4) (see Fig. 8). While the version 4.1 collection is improved over version 4 (Fig. 8), there appears to be remaining problems with the fPAR retrieval, particularly at low values, that have not been completely solved in the latest (v. 4.1) code.

Since a land cover map is used in the primary MODIS fPAR algorithms (Myneni et al., 2002; Tian et al., 2004), it is possible that the consistently high fPAR values after fire, result in part from applying a fixed biome value to this burnt chaparral site, and from the subsequent radiative transfer code that has biome-specific parameters. Because the dominant MODIS fPAR algorithm requires the use of look up tables for different biomes, this could easily be a source of error in fPAR derivation if the wrong biome classification were used. However, we examined this issue, and found that the biome classification, while originally incorrect for this site in version 4, was corrected to “open shrubland” for the version 4.1 fPAR retrieval, and probably not a significant source of error in this particular case. Thus, it seems likely that other steps in the radiative transfer code could be the source of the apparent overestimation of fPAR. It remains unclear whether this conclusion is a general one that can be applied to other ecosystems, or whether it reflects a characteristic of this particular site. Further work across a wide range of ecosystems would be needed to properly resolve this question.

Several studies have indicated that fPAR can be directly derived from NDVI without the need for ecosystem specific information such as biophysical or meteorological data (Gamon et al., 1995; Sims et al., 2006-this issue). Our study also demonstrates that using the backup algorithm for fPAR (an NDVI-driven algorithm) resulted in a MODIS fPAR values indistinguishable from that of ground measurements after fire (but note that this conclusion was gained for a single point indicated in Fig. 6). Consequently, we recommend a more extensive comparison of MODIS fPAR from different algorithms against ground based and aircraft measurements at a wider range of sites to evaluate sources of the continued disagreement between MODIS, AVIRIS and field-based fPAR measurements. To help evaluate fPAR retrievals and isolate the source of the apparent problem in the main MODIS fPAR algorithm, these comparisons should include a variety of ecosystem types and should also include extreme cases (e.g. complete snow cover or bare ground following fire), as these provide useful reference points with clearly definable conditions of low NDVI and fPAR.

A primary conclusion of this study is that continuous optical monitoring in the field with automated mobile spectrometers (tram system) provides an invaluable validation tool for MODIS products, revealing current strengths and weaknesses of these new satellite products. Furthermore, aircraft hyperspectral imagery (AVIRIS) provides an essential intermediate-scale tool for bridging the large gap in spatial scales that necessarily exist between satellite and field data. The excellent agreement between AVIRIS and tram data suggests that these two platforms provide reliable and coherent data suitable for ground

validation of satellite based measurements. The good agreement with EVI across all platforms, along with the fPAR disagreement, suggests that errors in MODIS products derive not from the instrument itself, but from the particular choice of algorithms used. Tram data provide continuous data at a relatively low cost needed for comparison with satellite or aircraft data, but are limited to relatively small regions (much smaller than a typical MODIS pixel). Aircraft hyperspectral imagery provides an ideal way to "bridge the gap" between such fine-scale data to the relatively coarse satellite data. Such systematic, multi-scale sampling, if adopted at additional ecosystems around the world, would greatly assist in understanding the strengths and weaknesses of current satellite products as a basis for improving these products.

Semi-arid sites such as this one, with their exposure to disturbance and large swings in productivity, provide robust tests of the behavior of different sensors and algorithms under a wider variety of conditions that is possible with relatively invariant sites. Similarly, further multi-scale tests across a diversity of ecosystems (e.g. Turner et al., 2005) would be particularly instructive. The SpecNet network (Gamon et al., 2006-this issue) provides an ideal starting point for such sampling.

Acknowledgements

This project was funded by three grants from the National Science foundation (CEA-CREST, NSF-Ecosystem and NSF-SGER) awarded to Dr. John Gamon. Thanks go to CEA-CREST funded students who helped in the data collection and tram construction, to SDSU field station program (especially Pablo Brant) for providing excellent technical and logistical support, to Hongyan Luo and Yonghai Qian from SDSU Global Change Research Group for assistance in field data collection, to Dr. Wenze Yang for assistance in providing/processing FPAR data of the site, to Dr. Fred Huemmrich for providing assistance in simulating MODIS bands and for suggestions on the manuscript. Thanks also go to the MODIS Land group and Oak Ridge DAAC who made the products available for this study site.

References

Aman, A., Randriamanantena, H. P., Podaire, A., & Frouin, R. (1992). Upscale Integration of Normalized Difference Vegetation Index—the Problem of Spatial Heterogeneity. *IEEE Transactions on Geoscience and Remote Sensing*, *30*, 326–338.

Chen, J. M. (1999). Spatial scaling of a remotely sensed surface parameter by contexture. *Remote Sensing of Environment*, *69*, 30–42.

Chen, J. M., Pavlic, G., Brown, L., Cihlar, J., Leblanc, S. G., White, H. P., et al. (2002). Derivation and validation of Canada-wide coarse-resolution leaf area index maps using high-resolution satellite imagery and ground measurements. *Remote Sensing of Environment*, *80*, 165–184.

Ehleringer, J. R., Bowling, D. R., Flanagan, L. B., Fessenden, J., Helliker, B., Martinelli, L. A., et al. (2002). Stable isotopes and carbon cycle processes in forests and grasslands. *Plant Biology*, *4*, 181–189.

Fensholt, R., Sandholt, I., & Rasmussen, M. S. (2004). Evaluation of MODIS LAI, fAPAR and the relation between fAPAR and NDVI in a semi-arid environment using in situ measurements. *Remote Sensing of Environment*, *91*, 490–507.

Gamon, J. A., Field, C. B., Goulden, M. L., Griffin, K. L., Hartley, A. E., Joel, G., et al. (1995). Relationships between NDVI, canopy structure, and photosynthesis in 3 Californian vegetation types. *Ecological Applications*, *5*, 28–41.

Gamon, J. A., Sims, D. A., Cheng, Y., Fuentes, D. A., Houston, S., & MacKinney, L. (2006). A mobile tram system for systematic ecosystem sampling of optical properties. *Remote Sensing of Environment*, *103*, 246–254 (this issue).

Gao, B. C., & Li, R. R. (2000). Quantitative improvement in the estimates of NDVI values from remotely sensed data by correcting thin cirrus scattering effects. *Remote Sensing of Environment*, *74*, 494–502.

Gao, Q., Yu, M., Yang, X. S., & Wu, J. G. (2001). Scaling simulation models for spatially heterogeneous ecosystems with diffusive transportation. *Landscape Ecology*, *16*, 289-+.

Gitelson, A. A. (2004). Wide dynamic range vegetation index for remote quantification of biophysical characteristics of vegetation. *Journal of Plant Physiology*, *161*, 165–173.

Goetz, A. F. H., Kindel, B. C., Ferri, M., & Qu, Z. (2003). HATCH: Results from simulated radiances, AVIRIS and Hyperion. *IEEE Transactions on Geoscience and Remote Sensing*, *41*, 1215–1222.

Green, R. O., Eastwood, M. L., Sarture, C. M., Chrien, T. G., Aronsson, M., Chippendale, B. J., et al. (1998). Imaging spectroscopy and the Airborne Visible Infrared Imaging Spectrometer (AVIRIS). *Remote Sensing of Environment*, *65*, 227–248.

Huemmrich, K. F., Privette, J. L., Mukelabai, M., Myneni, R. B., & Knyazikhin, Y. (2005). Time-series validation of MODIS land biophysical products in a Kalahari woodland, Africa. *International Journal of Remote Sensing*, *26*, 4381–4398.

Huete, A., Didan, K., Miura, T., Rodriguez, E. P., Gao, X., & Ferreira, L. G. (2002). Overview of the radiometric and biophysical performance of the MODIS vegetation indices. *Remote Sensing of Environment*, *83*, 195–213.

Huete, A., Justice, C., & Liu, H. (1994). Development of Vegetation and Soil Indexes for MODIS-EOS. *Remote Sensing of Environment*, *49*, 224–234.

Huete, A. R., Liu, H. Q., Batchily, K., & vanLeeuwen, W. (1997). A comparison of vegetation indices global set of TM images for EOS-MODIS. *Remote Sensing of Environment*, *59*, 440–451.

Keeley, J. E. (1992). Recruitment of seedlings and vegetative sprouts in unburned chaparral. *Ecology*, *73*, 1194–1208.

Knyazikhin, Y., Martonchik, J. V., Myneni, R. B., Diner, D. J., & Running, S. W. (1998). Synergistic algorithm for estimating vegetation canopy leaf area index and fraction of absorbed photosynthetically active radiation from MODIS and MISR data. *Journal of Geophysical Research-Atmospheres*, *103*, 32257–32275.

Lakshmi, V., & Zehrfuhs, D. (2002). Normalization and comparison of surface temperatures across a range of scales. *IEEE Transactions on Geoscience and Remote Sensing*, *40*, 2636–2646.

Lobo, A., Marti, J. J. I., & GimenezCassina, C. C. (1997). Regional scale hierarchical classification of temporal series of AVHRR vegetation index. *International Journal of Remote Sensing*, *18*, 3167–3193.

Marion, G. M., & Black, C. H. (1988). Potentially Available Nitrogen and Phosphorus Along a Chaparral Fire Cycle Chronosequence. *Soil Science Society of America Journal*, *52*, 1155–1162.

Miura, T., Huete, A. R., Yoshioka, H., & Holben, B. N. (2001). An error and sensitivity analysis of atmospheric resistant vegetation indices derived from dark target-based atmospheric correction. *Remote Sensing of Environment*, *78*, 284–298.

Myneni, R. B., Hoffman, S., Knyazikhin, Y., Privette, J. L., Glassy, J., Tian, Y., et al. (2002). Global products of vegetation leaf area and fraction absorbed PAR from year one of MODIS data. *Remote Sensing of Environment*, *83*, 214–231.

Myneni, R. B., Nemani, R. R., & Running, S. W. (1997). Estimation of global leaf area index and absorbed par using radiative transfer models. *IEEE Transactions on Geoscience and Remote Sensing*, *35*, 1380–1393.

Nemani, R. R., Keeling, C. D., Hashimoto, H., Jolly, W. M., Piper, S. C., Tucker, C. J., et al. (2003). Climate-driven increases in global terrestrial net primary production from 1982 to 1999. *Science*, *300*, 1560–1563.

Peddle, D. R., Johnson, R. L., Cihlar, J., & Latifovic, R. (2004). Large area forest classification and biophysical parameter estimation using the 5-Scale canopy reflectance model in Multiple-Forward-Mode. *Remote Sensing of Environment*, *89*, 252–263.

Rahman, A. F., Cordova, V. D., Gamon, J. A., Schmid, H. P., & Sims, D. A. (2004). Potential of MODIS ocean bands for estimating CO_2 flux from terrestrial vegetation: a novel approach. *Geophysical Research Letters*, *31*, L10503, doi:10.1029/2004GL019778.

Rahman, A. F., Gamon, J. A., Fuentes, D. A., Roberts, D. A., & Prentiss, D. (2001). Modeling spatially distributed ecosystem flux of boreal forest using hyperspectral indices from AVIRIS imagery. *Journal of Geophysical Research-Atmospheres*, *106*, 33579–33591.

Reich, P. B., Turner, D. P., & Bolstad, P. (1999). An approach to spatially distributed modeling of net primary production (NPP) at the landscape scale and its application in validation of EOS NPP products. *Remote Sensing of Environment*, *70*, 69–81.

Roberts, G. (2001). A review of the application of BRDF models to infer land cover parameters at regional and global scales. *Progress in Physical Geography*, *25*, 483–511.

Salomonson, V. V., & Appel, I. (2004). Estimating fractional snow cover from MODIS using the normalized difference snow index. *Remote Sensing of Environment*, *89*, 351–360.

Schimel, D. S., House, J. I., Hibbard, K. A., Bousquet, P., Ciais, P., Peylin, P., et al. (2001). Recent patterns and mechanisms of carbon exchange by terrestrial ecosystems. *Nature*, *414*, 169–172.

Sims, D. A., Luo, H., Hastings, S., Oechel, W. C., Rahman, A., & Gamon, J. A. (2006). Parallel adjustments in vegetation greenness and ecosystem CO_2 exchange in response to drought in a Southern California chaparral ecosystem. *Remote Sensing of Environment*, *103*, 289–303 (this issue).

Smith, J. A., & Ballard, J. R. (1999). Effect of spatial resolution on thermal and near-infrared sensing of canopies. *Optical Engineering*, *38*, 1413–1423.

Soegaard, H., Nordstroem, C., Friborg, T., Hansen, B. U., Christensen, T. R., & Bay, C. (2000). Trace gas exchange in a high-arctic valley 3. Integrating and scaling CO2 fluxes from canopy to landscape using flux data, footprint modeling, and remote sensing. *Global Biogeochemical Cycles*, *14*, 725–744.

Tian, Y., Dickinson, R. E., Zhou, L., Zeng, X., Dai, Y., Myneni, R. B., et al. (2004). Comparison of seasonal and spatial variations of leaf area index and fraction of absorbed photosynthetically active radiation from Moderate Resolution Imaging Spectroradiometer (MODIS) and Common Land Model.*Journal of Geophysical Research-Atmospheres* (109,-).

Tian, Y. H., Wang, Y. J., Zhang, Y., Knyazikhin, Y., Bogaert, J., & Myneni, R. B. (2003). Radiative transfer based scaling of LAI retrievals from reflectance data of different resolutions. *Remote Sensing of Environment*, *84*, 143–159.

Turner, D. P., Ritts, W. D., Cohen, W. B., Gower, S. T., Zhao, M. S., Running, S. W., et al. (2003). Scaling Gross Primary Production (GPP) over boreal and deciduous forest landscapes in support of MODIS GPP product validation. *Remote Sensing of Environment*, *88*, 256–270.

Turner, D. P., Ritts, W. D., Cohen, W. B., Maeirsperger, T. K., Gower, S. T., Kirschbaum, A. A., et al. (2005). Site-level evaluation of satellite-based global terrestrial gross primary production and net primary production monitoring. *Global Change Biology*, *11*, 666–684.

Wang, Q., Tenhunen, J., Falge, E., Bernhofer, C., Granier, A., & Vesala, T. (2004). Simulation and scaling of temporal variation in gross primary production for coniferous and deciduous temperate forests. *Global Change Biology*, *10*, 37–51.

Wu, Y. C., & Strahler, A. H. (1994). Remote Estimation of Crown Size, Stand Density, and Biomass on the Oregon Transect. *Ecological Applications*, *4*, 299–312.

Wythers, K. R., Reich, P. B., & Turner, D. P. (2003). Predicting leaf area index from scaling principles: corroboration and consequences. *Tree Physiology*, *23*, 1171–1179.

Xiao, X. M., Hollinger, D., Aber, J., Goltz, M., Davidson, E. A., Zhang, Q. Y., et al. (2004). Satellite-based modeling of gross primary production in an evergreen needleleaf forest. *Remote Sensing of Environment*, *89*, 519–534.